Thermodynamics of acicular ferrite nucleation

G. I. Rees and H. K. D. H. Bhadeshia

The thermodynamic driving force necessary to stimulate the nucleation of acicular ferrite and bainite is investigated for a series of high strength weld metals, using a combination of dilatometry, scanning electron microscopy, and thermodynamic calculations. The results indicate that the nucleation of acicular ferrite and bainite can be represented by the same thermodynamic model. It therefore appears that the nucleation mechanism of acicular ferrite on non-metallic inclusions in weld metals is essentially similar to that of bainite at the austenite grain boundaries. Metallographic observations confirm the notion that acicular ferrite is essentially intragranularly nucleated bainite.

MST/1897

© 1994 The Institute of Materials. *Manuscript received 23 April 1993; in final form 7 July 1993.* *The authors are in the Department of Materials Science and Metallurgy, Cambridge University/JRDC, Cambridge.*

Introduction

Acicular ferrite is believed to toughen welds and wrought steels by virtue of the fact that its microstructure consists of a rather chaotic arrangement of ferrite plates facing many different directions within any given austenite grain. Such an arrangement of plates can frequently deflect a propagating crack. This contrasts with the organised microstrucure of a packet of bainite plates, in which adjacent plates are not only parallel but in very similar crystallographic orientations in space. A cleavage crack can therefore propagate undeflected across the entire packet. Given its technological importance, it would be useful to be able quantitatively to model the development of the acicular ferrite microstructure as a function of steel chemistry and heat treatment. Previous efforts have relied on the fact that in many welds, the amount of acicular ferrite can be estimated by difference,[1] i.e. by setting it equal to the fraction of austenite that remains untransformed after allotriomorphic ferrite and Widmanstätten ferrite have formed. This is convenient because the fractions of these latter phases can be modelled accurately. However, there are many circumstances for which this method is likely to fail. In high strength welds where there is no allotriomorphic or Widmanstätten ferrite, the amount of acicular ferrite would, using the method of difference, always be estimated incorrectly as 100%. A model for acicular ferrite requires an understanding of its mechanism of formation. In this context, recent work has identified many important similarities between bainite and acicular ferrite. Thus, the microstructures are thought to form by an identical transformation mechanism, the morphological difference arising because bainite sheaves grow as a series of parallel platelets emanating from the austenite grain surfaces whereas acicular ferrite platelets nucleate intragranularly from point sites so that parallel formations of plates cannot develop. This theory is supported by the following observations, which are discussed in detail elsewhere.[2] The classic work of Ito *et al.*[3] demonstrates that acicular ferrite only forms below the bainite start temperature. The formation of both bainite and acicular ferrite leads to an invariant plane strain surface relief (with a large shear component)[4] and there is no substitutional solute partitioning during transformation.[5] Both reactions stop when the austenite carbon concentration reaches a value where displacive transformation becomes thermodynamically impossible.[4,6,7] There is a large and predictable hysteresis in the temperature at which austenite formation begins from a mixed microstructure of acicular ferrite and austenite, or bainite and austenite.[8] Any factor which enhances austenite grain surface nucleation relative to nucleation on inclusions stimulates bainite at the expense of acicular ferrite. For example, the removal of inclusions causes the microstructure to change from acicular ferrite to bainite.[9] Similarly, the elimination of austenite grain surfaces by decoration with inert allotriomorphic ferrite layers leads to a transition from bainite to acicular ferrite.[7] As with upper and lower bainite, it is also possible to find upper and lower acicular ferrite.[10] The purpose of the present work was to verify that the nucleation of acicular ferrite can be represented by the same thermodynamic method as has been applied successfully to bainite nucleation.

Mechanism of nucleation

It is found that both bainite and Widmanstätten ferrite evolve from the same nucleus, the nucleation process being displacive with only carbon partitioning during the nucleation stage. The nucleus is only able to grow into bainite when diffusionless growth (with an adequate allowance for the stored energy of bainite) can be sustained at the transformation temperature; otherwise Widmanstätten ferrite forms. This model is essentially based on martensite nucleation theory (except for the carbon partitioning);[11] the activation energy for nucleation is then predicted and found[12,13] to vary linearly with the chemical driving force. This behaviour contrasts with classical nucleation theory where the activation energy for nucleation is inversely proportional to some power of the chemical driving force. The linear dependence arises from the idea that undercooled austenite already contains pre-existing embryos. The nucleation event is the point where the embryos begin rapid growth. The activation energy is then the barrier to interface motion, which decreases approximately linearly as the chemical driving force increases. The exact mechanism for acicular ferrite nucleation is far from established although it is certain that the initial nucleation occurs heterogeneously at non-metallic inclusions present in the steel. A displacive nucleation mechanism requires the existence of a glissile interface between the nucleus and the matrix. It seems unlikely that the inclusion/austenite interface can in general be glissile and dissociate directly into an embryo of ferrite. This does not, however, make a displacive nucleation process impossible because the dislocation debris generated in the austenite adjacent to the inclusion, perhaps due to differential thermal expansion effects, could provide the necessary arrays which might dissociate into appropriate

embryos. Whatever the detailed issues at the inclusion/austenite interface, it would be extremely useful to be able to predict the acicular ferrite start temperature and experimentally access quantitative data on the thermodynamics of acicular ferrite nucleation. The design of the experiments can be based on the linear relationship discussed above, between the activation energy and the driving force. It can be demonstrated that this relationship in turn implies that the driving force at the transformation start temperature should vary linearly with the start temperature.[12] It is this latter relationship which is the basis of the experimental work presented below.

Experimental procedure

Dilatometric experiments for the measurement of transformation start temperatures were carried out using a Thermecmastor thermomechanical simulator (TMS) which has full computer control and computer data acquisition facilities. A series of submerged arc welds with systematic variations in deposit chemistry was provided by ESAB AB (Sweden). The mild steel base plates were 20 mm in thickness, the joints being of the all weld metal type ISO 2560 geometry, containing about 18 runs in three layers. The welding current was 500 A at 30 V, with a welding speed of 8 mm s^{-1} and an interpass temperature of 200°C. The compositions of these welds are given in Table 1. Samples for dilatometry were prepared by cutting sections parallel to the weld centreline from the innermost part of each weld, well away from the areas of possible base plate dilution. These sections were hot swaged down to rods of the appropriate diameter. After homogenisation for three days at 1200°C, in sealed quartz tubes, under a partial pressure of argon, the outer layer of the rods was removed to eliminate any oxidised or decarburised surface. All specimens were nickel plated in order to minimise the possibility of decarburisation during austenitisation and surface nucleation during transformation. The specimen diameter and length for the Thermecmastor were 6 and 12 mm respectively.

The time–temperature–transformation (TTT) diagram for steels consists essentially of two C-curves,[13] the high temperature curve representing reconstructive transformations such as allotriomorphic ferrite and pearlite. The lower C-curve represents the displacive transformations (Widmanstätten ferrite, bainite, and acicular ferrite). This curve has a flat top corresponding to the transformation start temperature. The alloys discussed above are designed to avoid the formation of Widmanstätten ferrite[14,15] so that the flat top of the lower C-curve corresponds to the bainite or acicular ferrite start temperature. Furthermore, the flat top permits the determination of the transformation start temperature using continuous cooling experiments, since the start temperature is simply that which does not change with two successively slower cooling rates.

Table 1 Compositions of alloys in high strength weld series, wt-% (bold numbers indicate the major changes in chemistry relative to alloy 112)

Alloy no.	C	Si	Mn	Cr	Mo	Ni	V
112	0·062	0·26	1·30	0·44	0·38	2·18	0·00
113	0·059	0·47	1·48	0·63	0·37	2·00	0·00
114	**0·079**	0·53	1·64	0·69	0·42	2·32	0·00
115	0·059	0·48	**2·02**	0·65	0·41	2·20	0·025
116	0·053	0·46	**1·08**	0·65	0·41	2·20	0·022
117	0·054	0·46	1·53	0·66	0·41	**3·01**	0·022
118	0·052	0·44	1·51	0·66	0·41	**1·52**	0·022
119	0·067	0·47	1·53	0·64	**0·57**	2·13	0·022
120	0·052	0·44	1·58	0·64	**0·24**	2·18	0·020
121	0·052	0·42	1·51	**0·90**	0·41	2·23	0·022
122	0·054	0·43	1·56	**0·36**	0·42	2·30	0·021

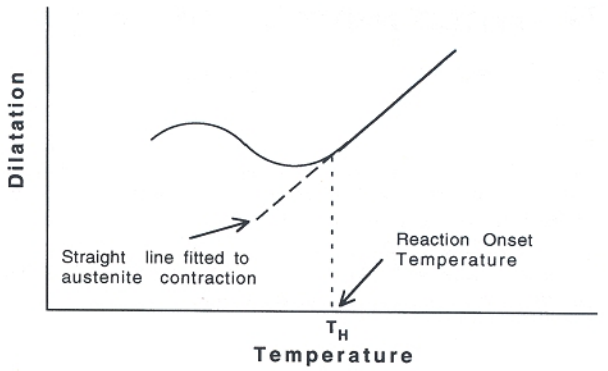

1 Schematic illustration of method for determining transfromation start temperature from dilatometric data

AUSTENITE GRAIN SIZE

Large austenite grains are required for the preferential formation of acicular ferrite relative to bainite.[6] An austenitisation treatment of 3 min at 1350°C was found to produce an austenite grain size easily sufficient for intragranular effects to dominate those originating at the austenite grain surfaces. The small austenite grain size necessary to stimulate the preferential formation of bainite was achieved by austenitising for 5 min at 1000°C in the TMS. Precautions were taken to minimise decarburisation. The specimen chamber was purged with argon gas three times before pumping down to $\sim 2 \times 10^{-2}$ Pa before the austenitisation treatment. In the case of the high temperature experiments with slower cooling rates, transformation was interrupted at an intermediate temperature in order to investigate the microstructure of the products formed at temperatures immediately below the start temperature. Using this method the location of transformation initiation could be determined more easily.

DETERMINATION OF START TEMPERATURE

Figure 1 shows schematically the procedure by which the transformation start temperature was determined. The linear contraction of austenite at higher temperatures indicates the absence of transformation. A straight line is fitted to this portion of the curve. Significant deviation from this straight line indicates the start temperature (in kelvin) of transformation T_H.

DRIVING FORCE FOR NUCLEATION

Theory and data discussed elsewhere[13] were used to calculate the values of ΔG_m, the maximum free energy change accompanying nucleation, for each of the alloys for which a transformation start temperature T_H had been measured. These results were used to construct plots of ΔG_m versus T_H for nucleation in the large and small austenite grained specimens, representing acicular ferrite and bainite respectively.

Results

Table 2 shows the transformation start temperatures T_H observed after the different austenitisation treatments. The temperatures given are the highest values observed during experiments with cooling rates between 5 and 0·5 K s^{-1} for the lightly alloyed members of the series and between 0·5

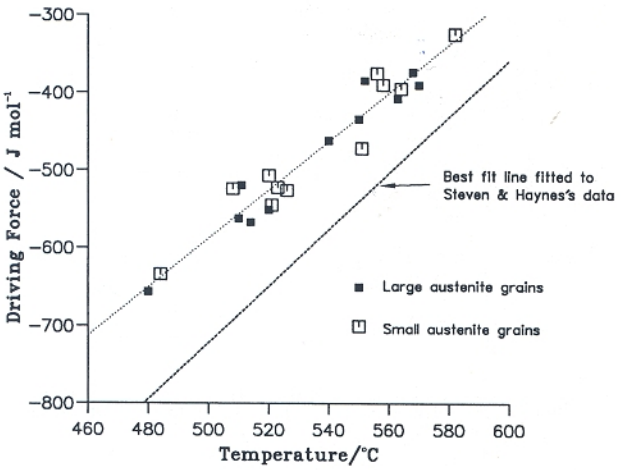

2 Plot of ΔG_m versus T_H for welding alloys studied, for transformation to bainite (small austenite grains) and acicular ferrite (large austenite grains) – best fit line through combined data is compared with overall relationship between ΔG_m and T_H for bainite nucleation determined by Ali and Bhadeshia[16] from data obtained by Steven and Haynes[17] indicating that welding alloys require somewhat lower driving force for nucleation

and 0·05 K s^{-1} for the more highly alloyed variants. It was verified in each case that this temperature did not change as the cooling rate was further decreased. The values of ΔG_m corresponding to the transformation start temperatures are also given in Table 2. A plot of ΔG_m versus T_H is shown in Fig. 2 which includes both the small and large austenite grain data. Best fit lines were determined for the relationship between T_H and the driving force ΔG_m available at these temperatures. The regression relationship for transformation to acicular ferrite (large austenite grain size) is

$$\Delta G_m\{T_H\} = 3{\cdot}112T_H - 2163 \text{ J mol}^{-1}$$

for T_H specified in °C. The correlation coefficient for the best fit straight line was 0·967. The standard errors for the regression coefficient and constant were 0·28 and 149 respectively. For transformation to bainite (small austenite grained samples), the corresponding regression relationship was found to be

$$\Delta G_m\{T_H\} = 3{\cdot}127T_H - 2153 \text{ J mol}^{-1}$$

which has a correlation coefficient of 0·97. In this case the standard errors in the regression coefficient and constant were 0·25 and 133 respectively. All the samples were examined using optical and scanning electron microscopy. Representative microstructures (Figs. 3–6) show the different microstructures formed during the cooling processes; the effect of alloy concentration is illustrated with the help of the high and low manganese variants 115 and 116.

Table 2 Transformation start temperatures T_H for small and large grained specimens, i.e. start temperatures for transfomation to bainite and acicular ferrite respectively (driving force at onset is also shown)

	$T_\gamma = 1000$°C		$T_\gamma = 1350$°C	
Alloy no.	T_H, °C	ΔG_m	T_H, °C	ΔG_m
112	563	−407	551	−472
113	550	−434	558	−390
114	510	−562	520	−507
115	480	−656	484	−634
116	570	−390	582	−325
117	511	−519	508	−524
118	568	−373	564	−395
119	520	−551	521	−545
120	552	−384	526	−526
121	514	−567	523	−522
122	540	−462	556	−375

T_γ austenitising temperature; ΔG_m maximum chemical free energy change available for nucleation.

It is interesting to note that both types of microstructure exhibit virtually identical best fit straight lines, despite the fact that the individual alloys show small changes in T_H following the different austenitisation treatments. There is no systematic trend in these small variations. Since the similarity between the regression equations for acicular ferrite and bainite formation is so great, a best fit straight line can be determined for the combined data. This expression is

$$\Delta G_m\{T_H\} = 3{\cdot}12T_H - 2148 \text{ J mol}^{-1}$$

The standard errors in the regression coefficient and constant are 0·18 and 95 respectively. Also noteworthy is the close agreement between the determined regression equations and that obtained by Ali and Bhadeshia[16] from the data of Stevens and Haynes[17]

$$G_N = 3{\cdot}636T_H - 2540 \text{ J mol}^{-1}$$

where G_N is the minimum driving force for detectable nucleation of displacive transformation. Here the standard errors for the regression and constant are 0·22 and 120 respectively. The small discrepancy between the two expressions, plotted in Fig. 2, suggests that it is somewhat easier to nucleate displacive transformations in the welding alloys than in the steels studied by Steven and Haynes. A possible reason for this is that the low carbon content of the alloys studied here results in a lesser degree of solid solution strengthening of austenite by carbon. A lower austenite yield strength would ease the motion of interface dislocations during displacive transformation.[11] This idea can be tested by isolating the lowest carbon steels used by Steven and Haynes for special consideration (*see* Table 3). It is interesting that the driving forces at the reported T_H temperatures of these steels are consistently lower than that predicted by the overall relationship between ΔG_m and T_H, determined by considering the complete set of steels, some of which contain much higher carbon concentrations. The best fit line determined for the driving force at T_H for these selected alloys is

$$\Delta G_m\{T_H\} = 3{\cdot}515T_H - 2420 \text{ J mol}^{-1}$$

with standard errors of 0·63 and 344 for the regression coefficient and regression constant respectively. Figure 7 plots ΔG_m versus T_H for these selected alloys, together with the best fit line through the data. For comparison, this figure also includes the best fit relationships between ΔG_m and T_H for both the combined acicular ferrite and bainite data determined in the present work, and for the complete set of alloys studied by Steven and Haynes, as discussed above. The curve for the selected low carbon alloys can be seen to lie between that determined for the welding alloys and that determined for all of the data obtained by Steven and Haynes. The degree of scatter about the best fit line for the selected alloys emphasises the close agreement between the relationship determined for the welding alloys with that determined for all of the data reported by Steven and Haynes.

It is known[18] that the solid solution strengthening of austenite by carbon is much more potent than that of substitutional solutes. It is therefore plausible that the effect of carbon should be particularly noticeable in the general class of low alloy steels of the type studied in the present work. Finally, it is worth emphasising that the observed linear relationship between the driving force at T_H, and T_H

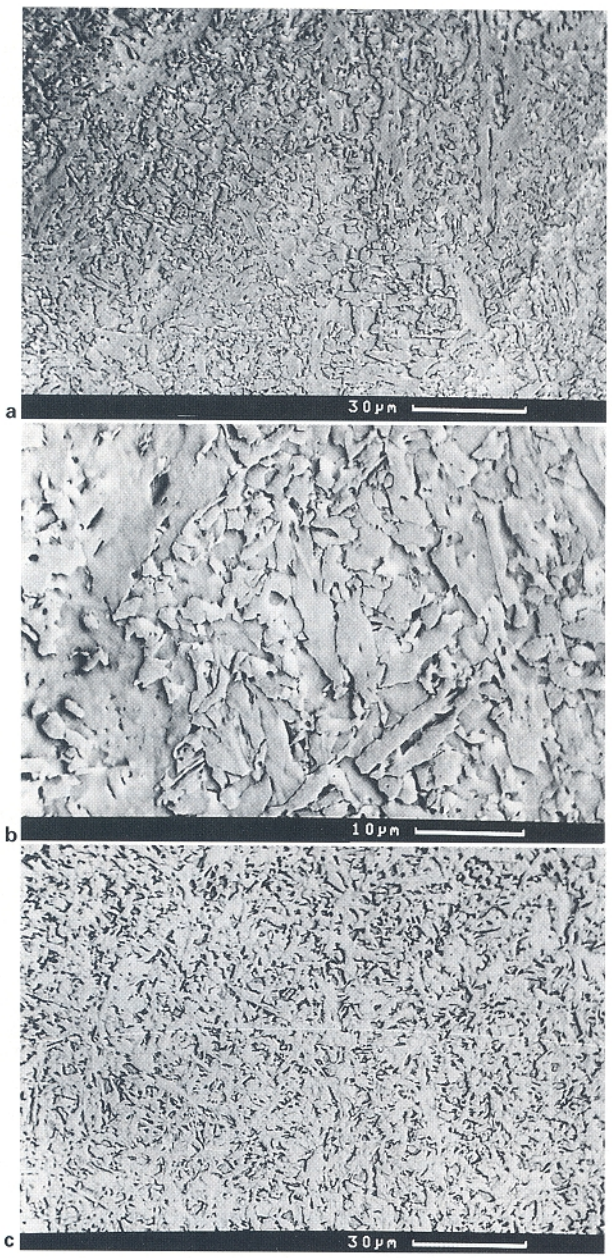

a low magnification image; *b* high magnification image showing acicular ferrite structure; *c* transformation interrupted by quenching at 450°C

3 Microstructure of alloy 116, austenitised for 3 min at 1350°C and cooled at *a*, *b* 5 K s^{-1} and *c* 0·5 K s^{-1}

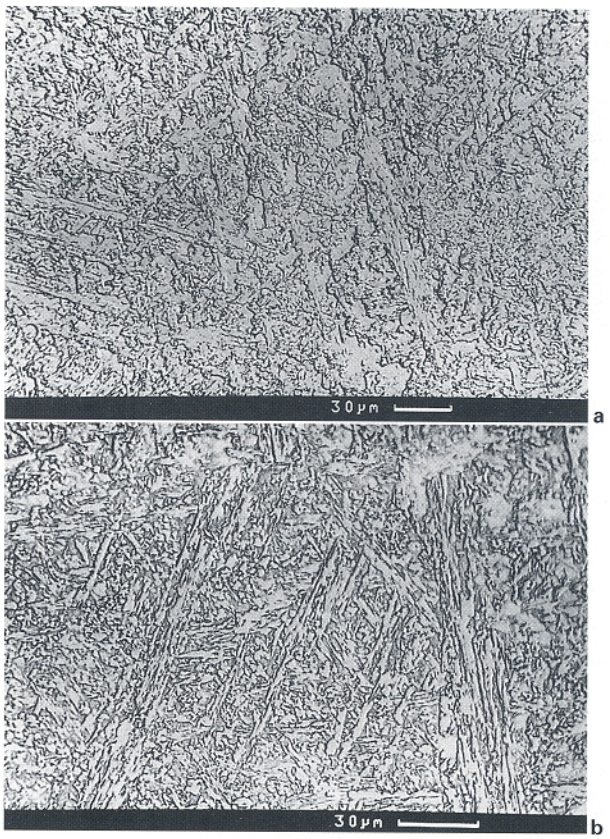

4 Microstructure of alloy 115, austenitised for 3 min at 1350°C and cooled at *a* 5 K s^{-1} and *b* 0·05 K s^{-1} (for *b* transformation was interrupted by quenching at 400°C)

for acicular ferrite amounts to a universal nucleation function for all low alloy steels. For the first time it allows the calculation of the acicular ferrite start temperature as a function of alloy chemistry. It could in principle also be used to estimate overall transformation kinetics in the manner currently undertaken for Widmanstätten ferrite and bainite.[19]

MICROSTRUCTURE

The micrographs of the large austenite grain size specimens are shown in Figs. 3 and 4; the samples austenitised at lower temperatures are shown in Figs. 5 and 6. Figures 3*a* and 3*b* show the microstructure of alloy 116 cooled to room temperature at 5 K s^{-1} after austenitisation at 1350°C. The higher magnification image clarifies the dense microstructure, showing the very high volume fraction of acicular ferrite. The same alloy, cooled more slowly and interrupted by quenching at 450°C, indicates the uniform formation of acicular ferrite plates (Fig. 3*c*). In comparison, the alloy 115 specimen cooled at 5 K s^{-1} indicates a greater tendency to form intragranularly nucleated sheaves (Fig. 4*a*) and displays a smaller fraction of transformation. Cooling alloy 115 at 0·05 K s^{-1} and interrupting the cooling by quenching from 400°C reveals very large sheaves surrounded by large regions of martensite as shown in Fig. 4*b*. In striking contrast to the large austenite grained specimens, the transformation of the finer austenite grains led invariably to a bainitic microstructure, which at the slowest of cooling rates had the appearance of classical 'granular bainite'. Granular bainite does not of course differ from conventional bainite in transformation mechanism, but is a morphological variant which is a consequence of the slow continuous cooling transformation.[20,21] Figure 5 shows the bainitic structures of alloy 116 cooled at 5 and 0·5 K s^{-1} respectively. The fraction of transformation is so high that it is difficult to identify individual sheaves. This is in contrast to the microstructures of the fine grained specimens of alloy 115 (Fig. 6) which revealed recognisable sheaves

Table 3 Alloy compositions and driving force values at T_H for lowest carbon alloys used by Steven and Haynes[17]

C	Si	Mn	Cr	Mo	Ni	T_H, °C	ΔG_m, J mol^{-1}
0·19	0·14	1·37	0·2	0·31	0·56	600	−348
0·14	0·19	0·46	1·11	0·12	3·55	550	−444
0·15	0·25	0·41	0·9	0·15	3·02	580	−362
0·11	0·21	0·3	0·13	0·3	5·04	550	−428
0·15	0·2	0·38	1·16	0·17	4·33	500	−634
0·14	0·22	0·5	2·00	0·18	2·13	520	−644
0·19	0·21	0·90	1·08	0·18	1·87	530	−617

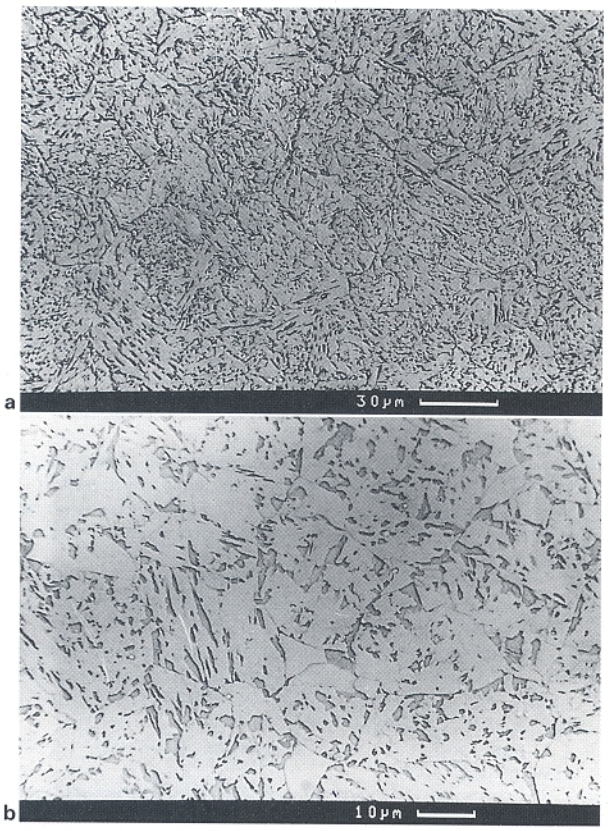

5 Microstructure of alloy 116, austenitised for 5 min at 1000°C and cooled at *a* 5 K s^{-1} and *b* 0·05 K s^{-1}

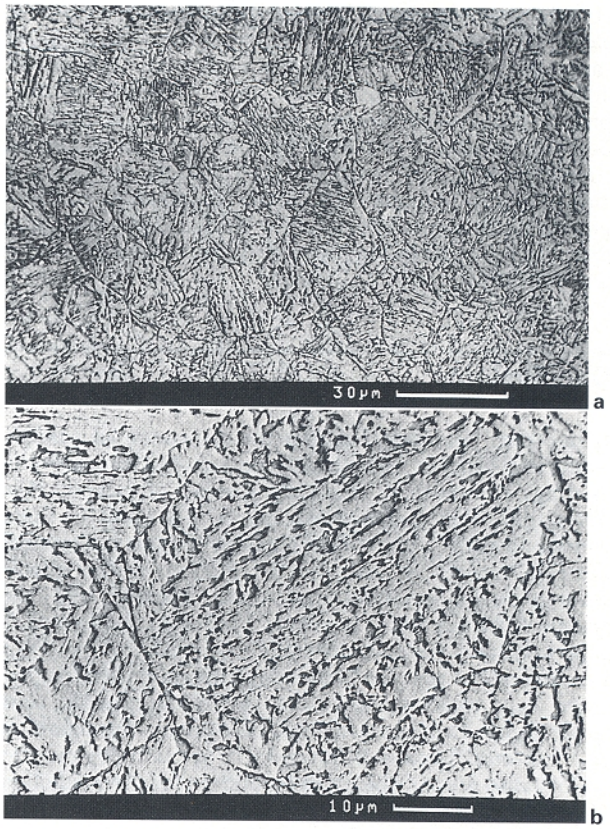

6 Microstructure of alloy 115, austenitised for 5 min at 1000°C and cooled at *a* 5 K s^{-1} and *b* 0·05 K s^{-1}

except the sample cooled at the slowest rate (0·05 K s^{-1}) which contained granular bainite. The regions of austenite which remain untransformed during bainite formation, which subsequently transform to martensite, are clearly more coarsely distributed in specimens which did not undergo predominantly intragranular nucleation (cf. Figs. 3*b* and 4*b*). These metallographic observations can be rationalised by considering the nucleation rates of the alloys during the early stages of transformation. In the coarse grained specimens the number density of grain boundary nucleation sites is insignificant compared with intragranular sites (inclusions) so that an acicular ferrite microstructure occurs. Superimposed on this austenite grain size effect is a distinct change in the acicular ferrite morphology as the austenite stabilising solute content of the alloy is increased. At the early stages of transformation, when the reaction driving force is small, the nucleation rate of acicular ferrite plates per unit volume is low, resulting in the probability of nucleation of plates on adjacent inclusions, and hence of impingement of these plates, being low. Thus, an opportunity exists for sheaves of acicular ferrite to develop from the inclusions, and this is exactly what is found (e.g. Fig. 4*b*). The effect of increasing cooling rate in any given alloy, on the development of the acicular ferrite microstructure is slightly different. By suppressing the transformation to larger undercoolings a more refined acicular ferrite microstructure is obtained (Fig. 4*a*). In the small grained specimens, the relatively large number density of austenite grain boundary nucleation sites results in the development of bainitic microstructures. It should be noted also that the formation of recognisable sheaves is more pronounced in the solute rich alloy 115. Granular bainite structures result from the condition in which the extent of transformation is always at its maximum allowable value during the slow cooling. The redistribution of partitioned carbon under these circumstances is enhanced, resulting in the obvious martensitic regions seen in the microstructures.

FURTHER WORK

The aim of the present work was to verify that the thermodynamics of acicular ferrite nucleation resembles that of bainite in ordinary steels. Therefore, the series of welds studied contains a substantial variation in the concentrations of alloying elements. They do not, however,

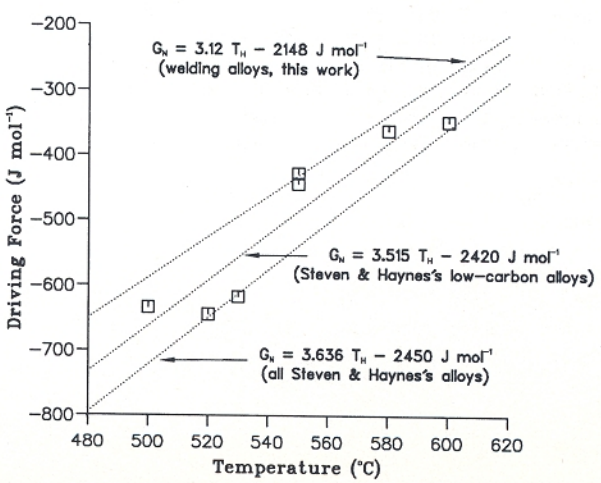

7 Plot of ΔG_m versus T_H for lowest carbon alloys studied by Steven and Haynes[17] – best fit line through data points is compared with relationship for acicular ferrite and bainite nucleation determined in present work, and with overall relationship determined for all alloys studied by Steven and Haynes[17]

contain any significant differences in inclusion forming elements since the design of the electrode coatings is the same for all the welds. The present work does not therefore address any issues about the potency of particular inclusion phases. Rather it establishes the nature of the relationship between the chemical driving force for nucleation and the transformation start temperature. Therefore, the effect of 'hardenability' changes on the start temperature has been proven to be identical to that for bainite. The problem of the effect of inclusion type requires investigation in future work.

Conclusions

It has been demonstrated that the nucleation of acicular ferrite is consistent with the assumption that there are pre-existing embryos in the supercooled austenite. The nucleation event then corresponds to the onset of rapid embryo growth. The activation energy for this operational nucleation event is that for the motion of the glissile embryo/matrix interface, and varies linearly with the chemical driving force. It follows from this, and indeed is experimentally verified, that the chemical driving force available at the acicular ferrite transformation start temperature itself varies linearly with the transformation start temperature. These experimental data enable the definition of a universal nucleation function (a function common to all low alloy steels) which can be utilised for the prediction of the acicular ferrite start temperature. It is exciting that the universal function for acicular ferrite nucleation on inclusions is found to be virtually identical to that of bainite in ordinary steels and in welding alloys. This verifies further that acicular ferrite is nothing but intragranularly nucleated bainite. But further, the similarity between the required driving force for nucleation of both transformations implies that an important role of inclusions might be to cause an appropriate disturbance in the adjacent austenite matrix, which causes the formation of arrays of dislocations in the austenite which may then dissociate to generate the necessary ferrite nuclei. Further work will be carried out to investigate this aspect in detail. Metallographic observations confirm that a reduction in the austenite grain size (i.e. an increase in the relative number density of grain surface to intragranular nucleation sites) promotes bainite at the expense of acicular ferrite, and vice versa. The fact that acicular ferrite sheaves develop from inclusions in highly alloyed steels where the driving force for transformation is reduced, supports the argument that it is impingement between plates nucleated on neighbouring inclusions which prevents sheaf formation in normal acicular ferrite microstructures.

Acknowledgements

The authors are grateful to Professor C. Humphreys for providing laboratory facilities, and to L.-E. Svensson and ESAB AB (Sweden) for funding the project. The contribution by one of the authors (HKDHB) was made as part of the Atomic Arrangement Design and Control project in association with the Research and Development Corporation of Japan.

References

1. H. K. D. H. BHADESHIA, L.-E. SVENSSON, and B. GRETOFT: *Acta Metall.*, 1985, **33**, 1271–1283.
2. H. K. D. H. BHADESHIA and L.-E. SVENSSON: 'Mathematical modelling of weld phenomenon', (ed. H. Cerjak and K. E. Easterling), 109–180; 1993, London, The Institute of Materials.
3. Y. ITO, M. NAKANISHI, and Y. KOMIZO: *Met. Constr.*, 1982, **14**, 472.
4. M. STRANGWOOD and H. K. D. H. BHADESHIA: 'Advances in welding science and technology', (ed. S. A. David), 209–213; 1987, Metals Park, OH, ASM.
5. M. STRANGWOOD: PhD thesis, University of Cambridge, 1987.
6. J. R. YANG and H. K. D. H. BHADESHIA: 'Advances in welding science and technology', (ed. S. A. David), 187–191; 1987, Metals Park, OH, ASM.
7. S. S. BABU and H. K. D. H. BHADESHIA: *Mater. Sci. Technol.*, 1990, **6**, 1005–1020.
8. J. R. YANG and H. K. D. H. BHADESHIA: 'Welding metallurgy of structural steels', (ed. J. Y. Koo), 549–563; 1987, Warrendale, PA, TMS.
9. P. L. HARRISON and R. A. FARRAR: *Int. Mater. Rev.*, 1989, **34**, 35–51.
10. A. A. B. SUGDEN and H. K. D. H. BHADESHIA: *Metall. Trans.*, 1989, **20A**, 1811–1818.
11. G. B. OLSON and M. COHEN: *Metall. Trans.*, 1976, **7A**, 1915–1923.
12. H. K. D. H. BHADESHIA: *Acta Metall.*, 1981, **29**, 1117–1130.
13. H. K. D. H. BHADESHIA: *Met. Sci.*, 1982, **16**, 156–165.
14. H. K. D. H. BHADESHIA and L.-E. SVENSSON: 'Improved weldment control using computer technology', 71–78; 1988, Oxford, Pergamon Press.
15. H. K. D. H. BHADESHIA and L.-E. SVENSSON: *J. Mater. Sci.*, 1989, **24**, 3180–3188.
16. A. ALI and H. K. D. H. BHADESHIA: *Mater. Sci. Technol.*, 1990, **6**, 781–784.
17. W. STEVEN and A. G. HAYNES: *J. Iron Steel Inst.*, 1956, **183**, 349.
18. K. J. IRVINE, D. T. LLEWELLYN, and F. B. PICKERING: *J. Iron Steel Inst.*, 1961, **199**, 153.
19. G. I. REES and H. K. D. H. BHADESHIA: *Mater. Sci. Technol.*, 1992, **8**, 985–993.
20. B. A. LEONT'YEV and G. V. KOVALEVSKAYA: *Fiz. Met. Metalloved*, 1974, **38**, 1050.
21. B. JOSEFSSON and H. O. ANDREN: *J. Phys.*, 1988, **49**, (11), 293–298.